Magnetic fluorescent bifunctional spin–crossover complexes

Jun–Li Wang, Qiang Liu, Xiao–Jin Lv, Rui–Lin Wang, Chun–Ying Duan and Tao Liu*

[1]*State Key Laboratory of Fine Chemicals, Dalian University of Technology, 2 Linggong Road, Dalian 116024, China.*

Correspondence and requests for materials should be addressed to L.T. (liutao@dlut.edu.cn)

Table S1. Selected bond angles (°) for $[Fe(L)_2(NCS)_2]$ at 282 K

Bond angles (°)			
N(1A)-Fe(1)-N(1)	180.0	N(1A)-Fe(1)-N(3A)	87.52(9)
N(1)-Fe(1)-N(3A)	92.48(9)	N(1A)-Fe(1)-N(3)	92.48(9)
N(1)-Fe(1)-N(3)	87.52(9)	N(3A)-Fe(1)-N(3)	180.0
N(1A)-Fe(1)-N(2A)	87.15(9)	N(1)-Fe(1)-N(2A)	92.85(9)
N(3A)-Fe(1)-N(2A)	74.51(8)	N(3)-Fe(1)-N(2A)	105.49(8)
N(1A)-Fe(1)-N(2)	92.85(9)	N(1)-Fe(1)-N(2)	87.15(9)
N(3A)-Fe(1)-N(2)	105.49(8)	N(3)-Fe(1)-N(2)	74.51(8)
N(2A)-Fe(1)-N(2)	180.00(9)		

Symmetry code A: –x + 1, –y + 1, –z + 1.

Table S2. Selected bond angles (°) for $[Fe(L)_2(NCS)_2]$ at 90 K

Bond angles (°)			
N(1A)-Fe(1)-N(1)	180.0	N(1A)-Fe(1)-N(3A)	87.05(6)
N(1)-Fe(1)-N(3A)	92.95(6)	N(1A)-Fe(1)-N(3)	92.95(6)
N(1)-Fe(1)-N(3)	87.05(6)	N(3A)-Fe(1)-N(3)	180.0
N(1A)-Fe(1)-N(2)	92.59(6)	N(1)-Fe(1)-N(2)	87.41(6)
N(3A)-Fe(1)-N(2)	104.43(6)	N(3)-Fe(1)-N(2)	75.58(6)
N(1A)-Fe(1)-N(2A)	87.41(6)	N(1)-Fe(1)-N(2A)	92.59(6)
N(3A)-Fe(1)-N(2A)	75.58(6)	N(3)-Fe(1)-N(2A)	104.43(6)
N(2)-Fe(1)-N(2A)	180.00(7)		

Symmetry code A: –x + 1, –y + 1, –z + 1.

Table S3. Selected bond angles (°) for $[Fe(L)_2(NCSe)_2]$ at 298 K

Bond angles (°)			
N(1A)-Fe(1)-N(1)	180.0	N(1A)-Fe(1)-N(3A)	85.38(8)
N(1)-Fe(1)-N(3A)	94.62(8)	N(1A)-Fe(1)-N(3)	94.62(8)
N(1)-Fe(1)-N(3)	85.38(8)	N(3A)-Fe(1)-N(3)	180.0
N(1A)-Fe(1)-N(2)	89.57(7)	N(1)-Fe(1)-N(2)	90.43(7)
N(3A)-Fe(1)-N(2)	105.20(6)	N(3)-Fe(1)-N(2)	74.80(6)
N(1A)-Fe(1)-N(2A)	90.44(7)	N(1)-Fe(1)-N(2A)	89.57(7)
N(3A)-Fe(1)-N(2A)	74.80(6)	N(3)-Fe(1)-N(2A)	105.20(6)
N(2)-Fe(1)-N(2A)	180.0		

Symmetry code A: – x + 1, – y + 2, – z + 1

Table S4. Selected bond angles (°) for $[Fe(L)_2(NCSe)_2]$ at 90 K

Bond angles (°)			
N(1)-Fe(1)-N(1A)	180.00(10)	N(1)-Fe(1)-N(3)	85.46(9)
N(1A)-Fe(1)-N(3)	94.54(9)	N(1)-Fe(1)-N(3A)	94.54(9)
N(1A)-Fe(1)-N(3A)	85.46(9)	N(3)-Fe(1)-N(3A)	180.00(10)
N(1)-Fe(1)-N(2)	90.06(8)	N(1A)-Fe(1)-N(2)	89.93(8)
N(3)-Fe(1)-N(2)	79.62(9)	N(3A)-Fe(1)-N(2)	100.38(9)
N(1)-Fe(1)-N(2A)	89.93(8)	N(1A)-Fe(1)-N(2A)	90.06(8)
N(3)-Fe(1)-N(2A)	100.38(9)	N(3A)-Fe(1)-N(2A)	79.62(9)
N(2)-Fe(1)-N(2A)	180.00(13)		

Symmetry code A: – x + 1, – y + 2, – z + 1

Table S5 Hydrogen bonding and π–π interactions [Å] at two temperatures for 1

Temperature	D–H···A	d(D···A)/Å	∠D–H···A/°
282 K	C5–H5···N6	2.998(4)	122.00
	C14–H14···S1B	3.270(3)	123.00
	C14–H14···N7	2.955(3)	109.00
	π···π	d(center···center)/Å 4.0506(18)	
90 K	C5–H5···N6	3.001(3)	121.00
	C14–H14···S1B	3.2075(19)	119.00
	C14–H14···N7	2.940(2)	110.00
	π···π	d(center···center)/Å 3.9738(12)	

Symmetry code B: x, y, – 1 + z

Table S6 Hydrogen bonding and π–π interactions [Å] at two temperatures for 2

Temperature	D–H···A	d(D···A)/Å	∠D–H···A/°
298 K	C5–H5···N6	3.042(3)	119.00
	C9–H9···N7	3.071(3)	113.00
	π···π	d(center···center)/Å	
		3.749(2)	
90 K	C2–H2···N4B	3.122(3)	142.00
	C5–H5···N6	3.061(3)	119.00
	C14–H14···Se1C	3.679(3)	133.00
	C14–H14···N7	3.032(4)	117.00
	π···π	d(center···center)/Å	
		3.6463(19)	

Symmetry code B: – x + 1, – y + 2, – z + 1; C: x, y – 1, z

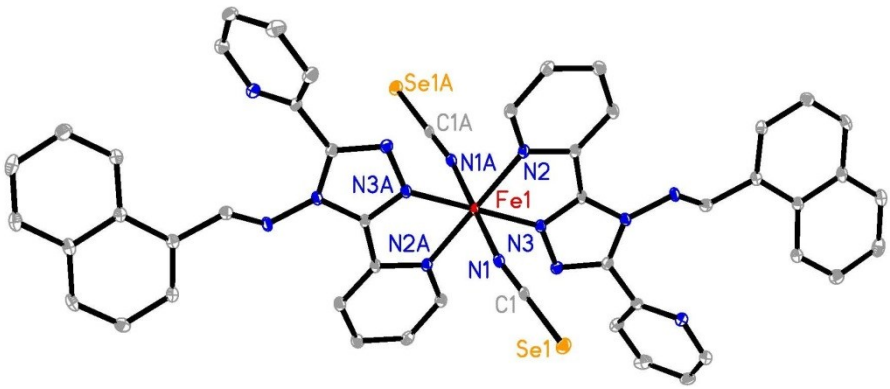

Fig. S1 ORTEP view of crystal structure of complex **2** at 90 K with the 30% probability thermal ellipsoid. Hydrogen atoms are omitted for clarity. Symmetry code A: –x + 1, –y + 2, –z + 1.

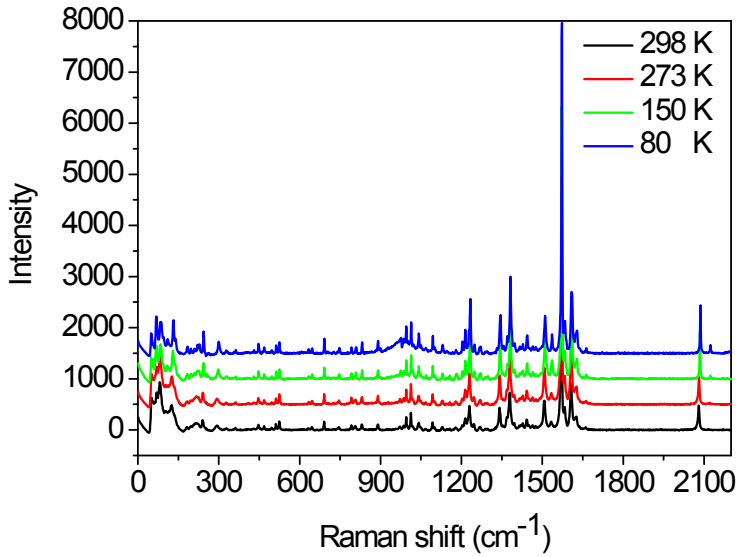

(a)

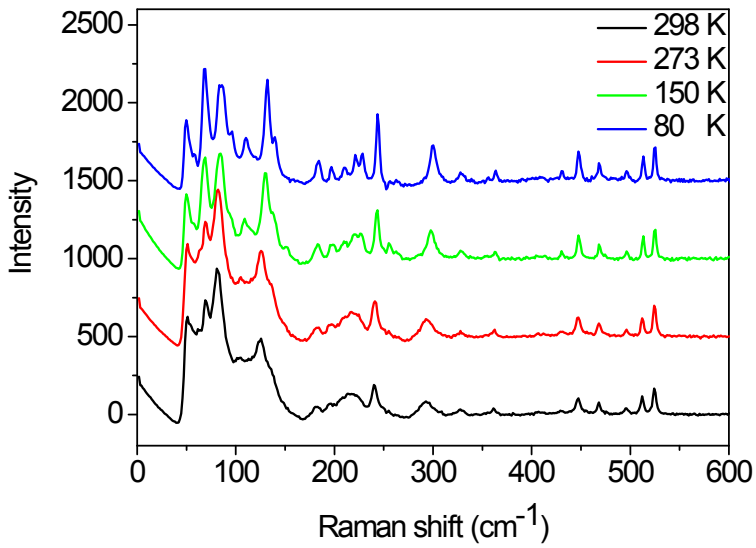

(b)

Fig. S2 Raman spectra (λ_{ex} = 633 nm) for **1** in wavenumber region 0–2200 cm^{-1} (a) and 0–600 cm^{-1} (b) at different temperatures.

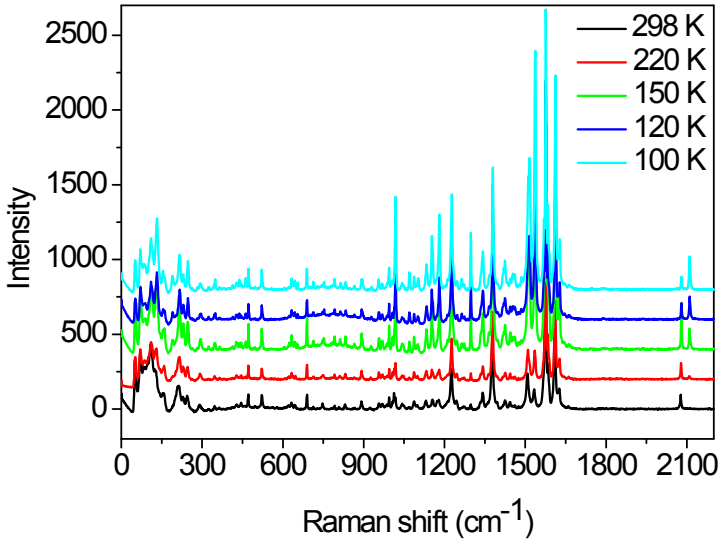

(a)

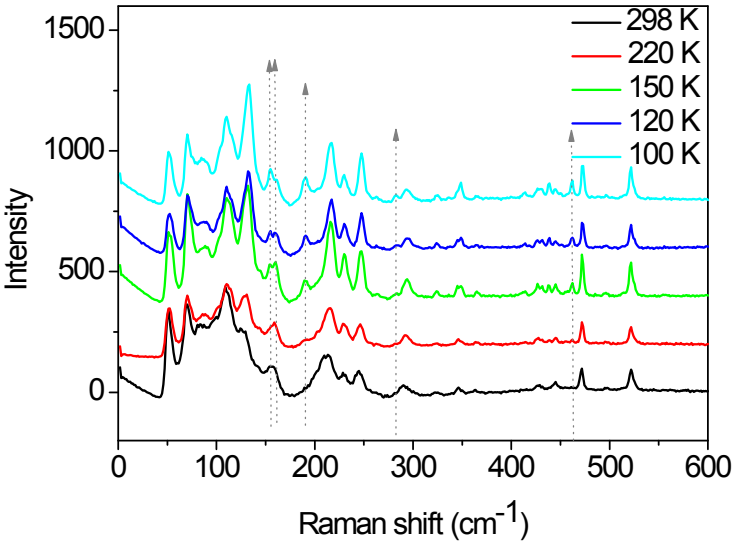

(b)

Fig. S3 Raman spectra (λ_{ex} = 633 nm) for **2** in wavenumber region 0–2200 cm^{-1} (a) and 0–600 cm^{-1} (b) at different temperatures.

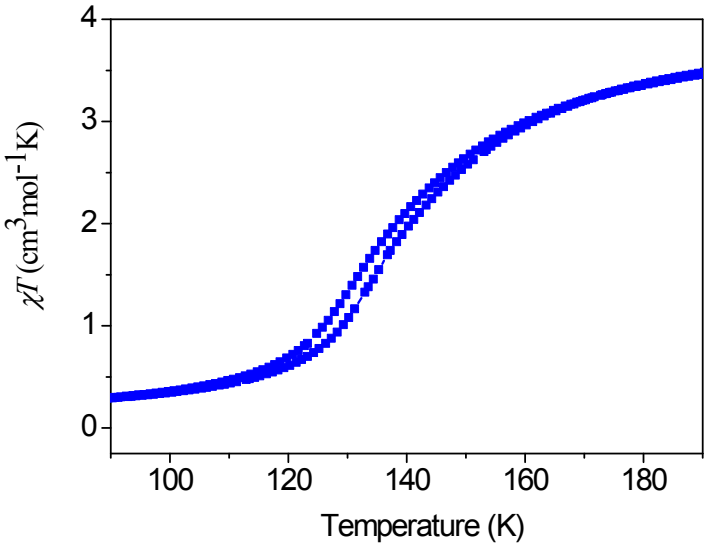

Fig. S4 Temperature dependence susceptibilities of complex **2** with a hysteresis loop before irradiation.

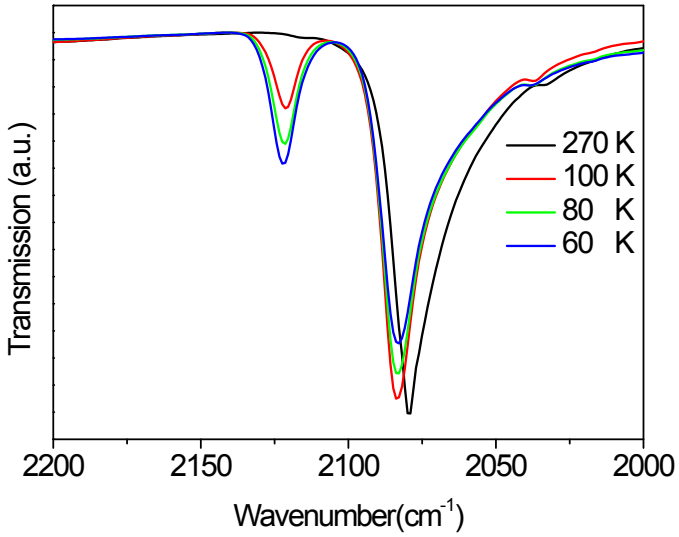

Fig. S5 Variable temperature solid state infrared spectra for **1** before irradiation.

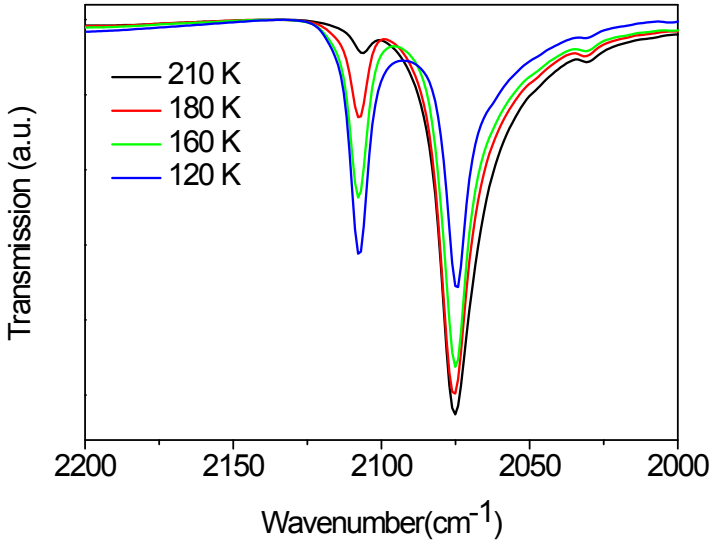

Fig. S6 Variable temperature solid state infrared spectra for **2** before irradiation.

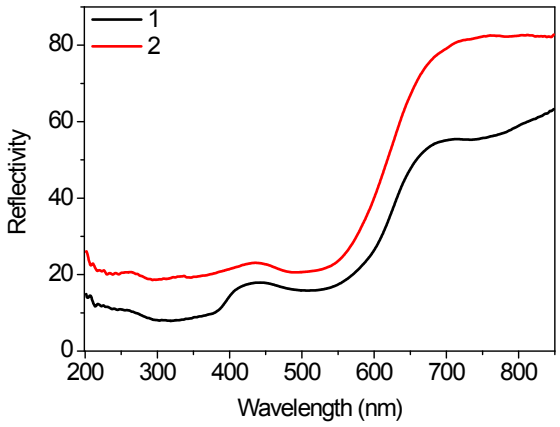

Fig.S7 Solid optical reflectivity spectra for **1** and **2.**

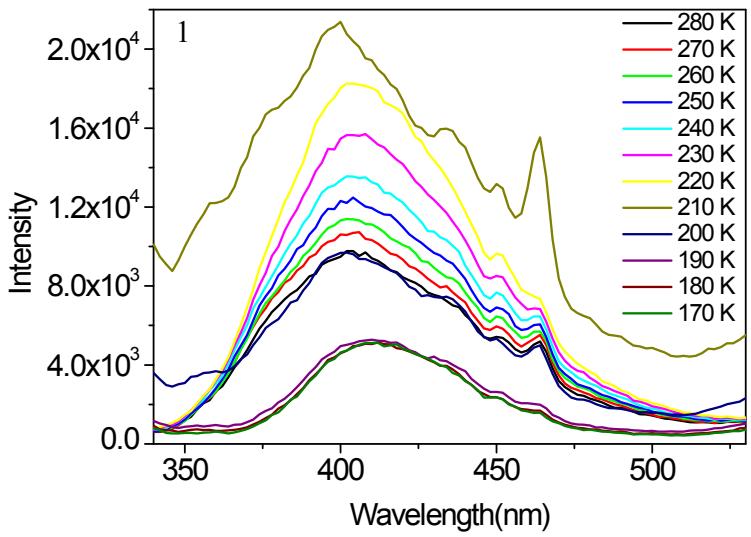

Fig.S8 Temperature-dependent fluorescence emission spectra between 280 K and 170 K for **1**.

Above 220 K, the fluorescence intensities exhibit a strong dependence on temperature. At 210 K, a drastic change is found in fluorescence spectrum shape, indicating glycol starts to solidify. The emission intensity drastically decreases at 200 K due to the weak transmission of light of glycol in solid state. The emission intensities mainly remain constant between 190 K and 170 K, indicative of the complete solidification of glycol.